Influence of a propulsive jet on the wake-flow structure of an axisymmetric space-launcher model

Anne-Marie Schreyer

Institute of Fluid Mechanics
TU Braunschweig
38108 Braunschweig, Germany
a.schreyer@tu-braunschweig.de
Current affiliation:
Institute of Aerodynamics, RWTH Aachen University, 52062 Aachen, Germany

ABSTRACT

We investigate the influence of an afterexpanding propulsive jet on the wake flow of a generic axisymmetric space-launcher model at a Mach number of $M = 2.9$ and a Reynolds number of $Re_D = 1.3 \cdot 10^6$, based on model diameter D. The description and discussion of turbulent structures in the wake flow, as well as the influence of a propulsive jet on their dynamic behavior is the focus of this study. The mean and turbulent flow topology and the dynamics of the wake are analyzed based on experimental data from Particle Image Velocimetry (PIV) measurements, Schlieren visualizations, and measurements of surface-pressure fluctuations. The data are interpreted with a combination of classical statistical analysis and post processing by means of Proper Orthogonal Decomposition (POD) and Dynamic Mode Decomposition (DMD). By combining the strengths of these different methods, we intend to improve the understanding of the mechanisms in the wake instability. In particular, we discuss the influence of the jet plume on the growth of vortices in the shear layer forming at the shoulder of the main body. Understanding this behavior will ultimately contribute to more efficient launcher designs and thus affordable access to space.

INTRODUCTION

The wake flow of a classical space launcher is dominated by the abrupt decrease in diameter at the junction between main body and rocket engine. At this discontinuity, the turbulent boundary layer on the main body separates, a shear layer starts to develop, and a large recirculation region forms downstream of the step. This separation-dominated flow field is highly unsteady and induces strong wall-pressure oscillations, which can excite structural vibrations detrimental to the launcher (Deprés *et al.* (2004)). The conditions and topology of the wake flow vary tremendously along the flight trajectory of the launcher. Especially the influence of the propulsive jet, which becomes increasingly underexpanded with altitude, has a strong influence. The afterexpanding jet plume has a strong displacement effect on the outer flow. This enlarges the recirculation region and causes an increase in pressure at the main-body base (Statnikov *et al.* (2016)). Depending on the conditions, the flow may not reattach on the nozzle fairing, potentially allowing hot exhaust gases from the engine nozzle to be convected upstream and harm the structure. Understanding this flow field is thus crucial to minimize those detrimental effects.

A number of studies describe the mean flow topology and base-pressure fluctuations, investigate the sources of these pressure disturbances, or observe the formation of turbulent structures in the wake for a range of conditions, see for example Deprés *et al.* (2004); Deck & Thorigny (2007); Bourdon & Dutton (1999); Statnikov *et al.* (2016). In the current study, we deepen our previous work on supersonic launcher-wake flow (Schreyer *et al.* (2016*b*,*a*)), by extracting the most energetic turbulent structures from our PIV data by means of POD, analyzing the dynamics of the recompression shock with DMD, and by discussing these results in conjunction with surface-pressure measurements, which represent the footprints of the turbulent structures in the wake. This combined approach provides better access to the mechanisms in the flow field.

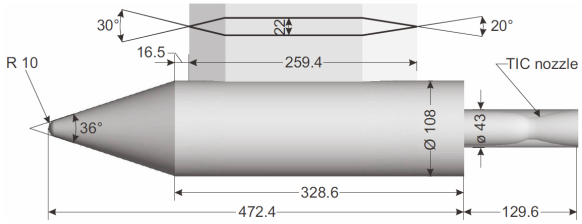

Figure 1: Sketch of the generic launcher model (dimensions in mm). Figure from Statnikov *et al.* (2016).

EXPERIMENTAL SETUP AND CONDITIONS

We study the wake of the generic axisymmetric space-launcher model shown in Figure 1 for a baseline case without propulsive jet and a jet-simulation case with an unheated air jet. Experimental investigations were performed in the Hypersonic Ludwieg tube Braunschweig in supersonic configuration at a flow Mach number of 2.9 and a Reynolds number $Re_D = 1.3 \cdot 10^6$ based on model diameter D. This corresponds to a simulated trajectory point at 25 km altitude. The nozzle exit velocity of the jet is at Mach 2.5, and the nozzle to freestream pressure ratio $p_e/p_\infty = 5.7$.

Particle Image Velocimetry (PIV) measurements were performed in a vertical plane on the opposite side of the strut support ($\theta = 180°$, bottom side of the model) to reduce disturbances induced by the support. A Litron Nano T180-15 PIV double-pulse Nd-YAG laser with a pulse energy of 150 mJ was used as light source. Two LaVision Imager Pro X 11M cameras with 4008×2672 pixels CCD chips and Tamron SP AF 180 mm F3.5 macro lenses were used to record the PIV images. In order to achieve a satisfactory spatial resolution and still observe a sufficiently large part of the wake-flow region, the flow field was split up into two fields of view. Oil droplets of the temperature resistant lubricant oil Plant Fluid were used to seed the outer flow, yielding a mean droplet size just below 200 nm. The seeding droplets were introduced into the wind-tunnel storage tube prior to each wind-tunnel run. See Schreyer *et al.* (2016*b*) for details.

Three Kulite XCS-093 pressure sensors with a pressure range of 0.35 bar absolute are flush-mounted into the main body base at a radial position of $r/D = 0.42$ at different angles ($\theta = 180°, 190°$, and $240°$). Two additional sensors with the same pressure range are placed along the nozzle fairing within the separation zone

($x/D = 0.31$) and at the reattachment location for the baseline case ($x/D = 0.77$). The pressure data were sampled with a Spectrum M2i.4652 transient recorder at a sampling frequency of 3 MHz. Fluctuations under 200 Hz and above the cut-off frequency of the pressure sensors at 50 kHz were removed by filtering.

Schlieren images were taken in a single-mirror coincident setup, using a mercury-vapor lamp as light source. A sequence of images with an exposure time of 1.5 μs was recorded with a Phantom v711 high-speed camera at a recording frequency of 22006 fps.

DATA ANALYSIS

Proper Orthogonal Decomposition (POD) (Berkooz *et al.* (1993)), in particular Snapshot-POD (Sirovich (1987)), is a method to extract coherent structures from (experimental and numerical) turbulence data, and is here applied to PIV data. The obtained spatial structures are sorted by energy content, and already a small number of POD modes can capture the energy content of flows like the shear layer we intend to study.

Dynamic mode decomposition (DMD) (Schmid (2010); Schmid *et al.* (2011); Jovanović *et al.* (2014)) allows for a modal analysis of a data sequence without requiring an underlying model, which makes it suitable for experimental data. The resulting modes represent the dominant dynamic behavior captured in the snapshots. DMD allows to extract dynamically relevant and coherent structures, providing both their spacial shape and characteristic frequency. Time-resolved PIV measurements are unattainable in supersonic flows; we apply DMD to temporally resolved sequences of Schlieren snapshots in this study (as demonstrated by Schmid *et al.* (2011)), and characterize the motion of the reattachment shock.

RESULTS AND DISCUSSION

Flow topology

To get an overview of the influence of the afterexpanding jet on the flow organization, averaged Schlieren images are shown in Figure 2, and sample PIV results are presented in Figure 3 for both cases. The boundary layer on the launcher main body separates at the shoulder and an expansion fan is forming. A shear layer develops and is deflected towards the afterbody surface, where it is then reflected. The geometric constraints lead to another deflection of the flow into the direction parallel to the nozzle surface and the consecutive formation of recompression waves. For the case without propulsive jet, a large separated zone is forming downstream of the main-body shoulder, and the flow is reattaching downstream on the nozzle fairing. Under the influence of the jet plume, the separated region is increased and reattachment does not occur anymore (see stream traces in Figures 3(a) and 3(b), see also e.g. Statnikov *et al.* (2016); Schreyer *et al.* (2016*b*)).

The jet plume appears to have a stabilizing effect on the wake flow, as indicated by the subdued development of the shear layer and the reduced magnitude of the turbulent intensities (compare Figures 3(c) and 3(d)). See Schreyer *et al.* (2016*a*) for a more detailed discussion. Deprés *et al.* (2004) suggested that this behavior can be observed since the jet obstructs the growth of the vortices in the shear layer.

Propulsive-jet influence on vortical structures

Such coherent vortical structures in turbulent flow typically contain a large fraction of the turbulent kinetic energy, which makes POD a suitable technique to detect those structures (see Berkooz *et al.* (1993)). For this purpose, we apply the more suitable Snapshot-POD (Sirovich (1987)) to the non-time-resolved PIV measurements in this study. Based on this decomposition, we intend to clarify whether or not the stabilizing effect that the propulsive jet

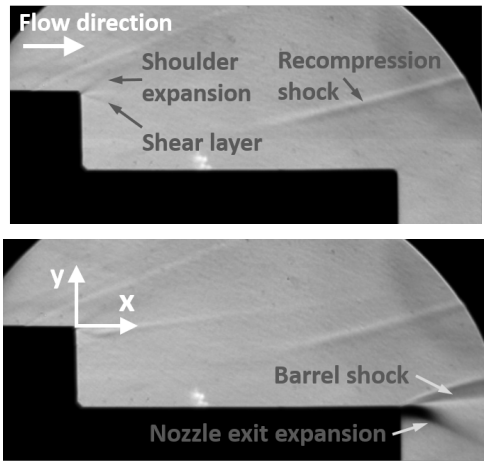

Figure 2: Schlieren visualizations (averaged from 400 snapshots). Top: baseline case, bottom: with propulsive jet.

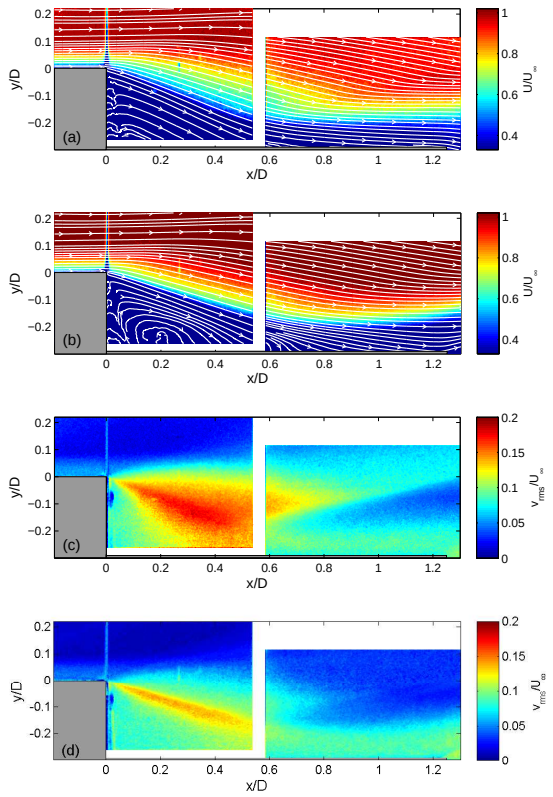

Figure 3: Contours of the normalized mean velocity component U/U_∞ in the main flow direction ((a) and (b)) and of the normalized turbulent fluctuation component v_{rms}/U_∞ in the radial direction ((c) and (d)) from PIV. (a) and (c): baseline case, (b) and (d) with propulsive jet. Figure from Schreyer *et al.* (2016*b*)

exerts on the wake is indeed effected by the presence of the jet limiting the growth of the turbulent structures.

The energy content in the respective eigenmodes, as well as the cumulative energy content after a number of n modes is presented in Fig. 4. The eigenmodes are sorted by decreasing fractional energy. The eigenspectra for both cases show one rather dominant mode. However, a significant fracture of the turbulent kinetic energy is

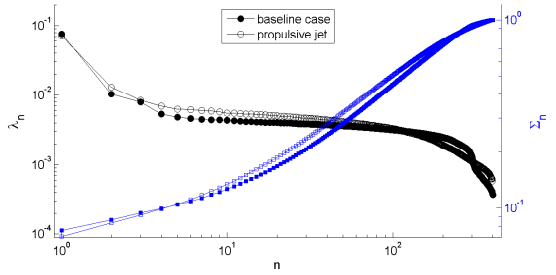

Figure 4: Eigenspectra λ_n and cumulative relative energy $\sum_n$ in the first n modes.

contained in a larger number of higher-order modes contributing to the dynamic behavior of the wake flow.

The first four weighted eigenmodes $\phi_{x,1}$ - $\phi_{x,4}$ representing normalised streamwise velocity fluctuations for the baseline and propulsive-jet cases are shown in Fig. 5 left and right, respectively. In both cases, the respective first eigenmodes are the most energetic modes and of comparable strength, containing 8% and 7% of the total kinetic energy, respectively. This mode represents streamwise velocity fluctuations within the separated shear layer. In the presence of a propulsive jet, the extent of this mode in the radial direction is slightly smaller than in the baseline case, and it extends further downstream. This agrees with the previously observed displacement of the shear layer away from the wall effected by the afterexpanding jet plume. The associated flatter shear-layer impingement angle on the nozzle fairing leads to weaker recompression waves and a slower, uncompleted reattachment process. The shear layer can develop over a longer downstream distance, but is restricted in its radial extent due to the influence of the jet plume.

The second to fourth modes show large alternating regions of streamwise velocity fluctuations, mainly located in the recirculation zone, the reattachment region, and the redeveloping boundary layer on the nozzle surface. In the baseline case without propulsive jet, the reattachment and realignment zone downstream of the separation bubble has a pronounced energy content. With propulsive jet, the region further downstream towards the nozzle exit contains more energy, as do the recirculation zone and separated shear layer in mode 4. This may indicate that in the propulsive-jet case, the vortex shedding from the shear layer is dominant, while the reattachment and redeveloping boundary layer on the nozzle surface seems more important in the baseline case (mode 4).

The differences between the two cases are more pronounced in the eigenmodes representing normalised velocity fluctuations in the radial (wall-normal) direction, shown in Fig. 6. Intermediate eigenmodes showing the same fundamental features are not shown. The first mode $\phi_{y,1}$ represents wall-normal velocity fluctuations in the shear layer and recirculation bubble in both cases. The influence of the displacement effect of the afterexpanding jet plume is visible in an additional vertical fluctuation component just upstream of the nozzle exit, as well as a reduced downstream extent of the mode component associated with vertical fluctuations in the shear layer (compare Figures 6(a) and (b)). For the baseline case, the third and fourth modes $\phi_{y,3}$ and $\phi_{y,4}$, respectively, contain a significant amount of energy in the location of the recompression shock. This represents the low-frequency shock oscillation typical for shock-wave boundary layer interactions with separation bubbles. In consistence with the previous finding that reattachment does not occur in the propulsive-jet case, this mechanism does not appear in the most dominant POD modes for this case (see Fig. 6 (right)). In higher-order modes ($\geq \phi_{y,3}$) of the baseline case, another significant fraction of the overall kinetic energy is contained within the reattaching and redeveloping boundary layer, as well as in the reattachment zone ($\frac{x}{D} \approx 0.7$). Modes of alternating upwards and downwards velocity fluctuations downstream of the reattachment location are probably linked to both vortices from within the shear layer, and vortices shed from the separation bubble in connection with the low-frequency shock unsteadiness typical for shock wave / boundary layer interactions (see for example Clemens & Narayanaswamy (2014)). Under the influence of the propulsive jet, the spatial representation of the higher-order modes ($\geq \phi_{y,3}$, Fig. 6 (right)) is represented by smaller and smaller zones of alternating velocity fluctuations. These are continuously located along the shear layer shed from the main-body shoulder and downstream along the nozzle surface. Therefore, and since no relevant fraction of the energy seems to be related to the motion of the recompression shock, we assume that these modes are related to the vortices from the shear layer, decaying into ever smaller structures. These small-scale velocity fluctuations still occupy a considerable fraction of the overall kinetic energy (see Fig. 4). Without jet, observed structures are of larger streamwise extent than in the correspondingly dominant modes in the propulsive-jet case.

The observed behavior suggests that the wake instability in the baseline case is associated with both the shear layer shed from the shoulder of the main body, probably influenced by the varying strength of the expansion fan, and the flow reattachment and instability of the recompression process. In the case with propulsive jet on the other hand, the reattachment process is weaker and incomplete, and therefore the wake instability appears to be mainly associated with the shear layer instability. The growth of structures in this shear layer, however, is restricted by the smaller width of the shear layer.

The observed dominance of dynamic motion in the radial direction is in agreement with the findings of Statnikov *et al.* (2015), who described flapping and swinging motions of the shear layer as dominant dynamic mechanisms in wake flows with afterexpanding propulsive jet.

Dynamic motion of the reattachment shock

Since the reattachment and recompression processes apparently contribute to the wake instability in a varying degree for the two observed cases, we attempted to investigate the dynamic motion of the reattachment shock. For this purpose, 400 Schlieren snapshots per case, equispaced in time with a delay of $dt = 45.4\,\mu$s (allowing to resolve Strouhal numbers St_D from 0.03 to 1.3), have been processed with DMD. The Strouhal number $St_D = \frac{f \cdot D}{U_\infty}$ was calculated based on the main-body diameter D. The sampling interval was chosen to allow the extraction of the typical low-frequency motion of shock waves associated with large-scale separation, and to match the resolution of the pressure sensors. Note that due to the nature of the Schlieren images, this is not an investigation of the complete dynamic behavior of the wake flow, as would be possible by applying DMD to time-resolved PIV or numerical data.

Representative DMD modes resulting from those investigations are shown for the two studied cases in Figure 7. The presented modes are the most dominant ones found in our DMD analysis on the density-based signal of the flow and represent the motion of the recompression shock. Several modes in a Strouhal number range of $0.04 \leq St_D \leq 0.08$ and $0.03 \leq St_D \leq 0.11$ for the baseline and propulsive jet cases, respectively, contribute to this motion. This is a typical observation for such flow fields (see Grilli *et al.* (2012)). The most prominent influence of the jet plume on the DMD modes is the apparent coupling between the motion of the recompression shock and the barrel shock and nozzle-exit expansion for the propulsive-jet case. In the baseline case, the dynamics of the recompression shock are most probably related to the motion of the separation zone. A

complete discussion of the low-frequency shock-oscillation mechanism in the present axisymmetric case is unfortunately not possible without insight into the separation region.

Footprint on the wall-pressure signal

The power spectral density (PSD) of the wall-pressure fluctuations gives complementary information about the dynamic behavior of the wake, since the base pressure signal represents a footprint of the turbulent structures in the wake (Deprés *et al.* (2004)). We will mainly discuss the low-frequency part of the pressure signal, which is critical with respect to potentially detrimental structural vibrations. The PSD shown in Fig. 8 was computed with Welchs method and is based on time traces of 30 ms. Hamming windows of 90,000 points and at 50% overlap were used for segmentation.

In the baseline case, the base pressure spectrum ($\phi = 180°$) features a characteristic elevated frequency range for a Strouhal number of around $St_D = 0.2$. This intensity maximum, attributed to vortex shedding from the separation bubble, is governed by interactions of structures formed in the shear layer with the wall in the reattachment region (Deprés *et al.* (2004)). It is observed for Mach numbers from the transonic to the hypersonic regime (see e.g. Deck & Thorigny (2007); Schreyer *et al.* (2016*a*); Statnikov *et al.* (2016)). The peak is followed by a steady decay until $St_D \approx 2$. Under the influence of the afterexpanding jet, this maximum is much less pronounced and shifted to a slightly higher Strouhal number. The low-frequency content is generally elevated and broadband. This agrees with the observation of a flatter shear-layer impingement angle on the nozzle surface, and thus a weaker interaction of the structures with the wall. In the baseline case, a very weak maximum for $St_D = 0.2$ can still be observed at $\frac{x}{D} = 0.31$ on the nozzle surface. This measurement location is still within the separation region, and the signal therefore contains contributions from the vortex-surface interactions described above. Further downstream, at $\frac{x}{D} = 0.77$, the $St_D = 0.2$ maximum has disappeared. The signal now features an elevated broadband low-frequency energy content. In both measurement locations on the nozzle, no influence of the propulsive jet on the PSD can be observed.

CONCLUSIONS

We studied the influence of an afterexpanding propulsive jet on the wake flow of a generic axisymmetric space-launcher model at a Mach number of $M = 2.9$ and a Reynolds number of $Re_D = 1.3 \cdot 10^6$. Our particular interest was the behavior of turbulent structures in the wake flow. Previous studies observed that the presence of a propulsive jet has a stabilizing effect on the wake. This particularly manifests itself in lower turbulent intensities of the velocity components in the near wake. Several reasons contribute to this stabilizing effect: The width of the shear layer is restricted by the displacement effect exerted by the jet plume and the outer flow. This restricts the maximum size of the vortices in the shear layer. Due to the displacement of the shear layer away from the wall, the shear layer develops for a longer streamwise distance, and the vortices decay into smaller structures. Furthermore, the displacement leads to a flatter impingement angle of the shear layer on the nozzle surface. Therefore, the reattachment process is slower and not completed along the length of the nozzle of our model. The reattachment and the unsteadiness of the recompression shock thus have a much smaller influence than in the baseline case. In our opinion, this last mechanism is the most important contribution to the observed effect.

ACKNOWLEDGEMENTS

Financial support from the German Research Foundation (DFG) in the framework of the SFB TRR 40 is gratefully acknowledged by the author.

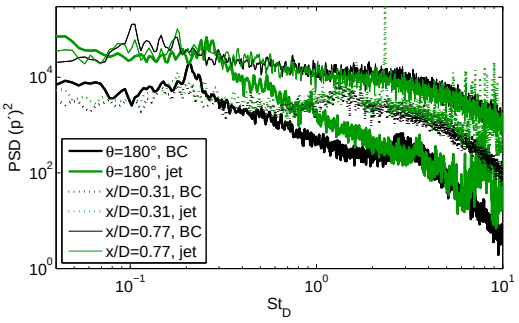

Figure 8: Power spectral density (PSD) of the pressure signals at the main-body base ($\theta = 180°$) and on the nozzle fairing for the baseline (BC) and propulsive jet (jet) cases.

REFERENCES

Berkooz, G., Holmes, P. & Lumley, J. L. 1993 The proper orthogonal decomposition in the analysis of turbulent flows. *Annual Review of Fluid Mechanics* **25**, 539–575.

Bourdon, C. J. & Dutton, J. C. 1999 Planar visualizations of large-scale turbulent structures in axisymmetric supersonic separated flows. *Physics of Fluids* **11** (1), 201–213.

Clemens, N. T. & Narayanaswamy, V. 2014 Low-Frequency Unsteadiness of Shock Wave/Turbulent Boundary Layer Interactions. *Annual Review of Fluid Mechanics* (46), 469–492.

Deck, S. & Thorigny, P. 2007 Unsteadiness of an axisymmetric separating-reattaching flow: Numerical investigation. *Physics of Fluids* **19** (6), –.

Deprés, D., Reijasse, P. & Dussauge, J.-P. 2004 Analysis of Unsteadiness in Afterbody Transonic Flows. *AIAA Journal* **42** (12), 2541–2550.

Grilli, M., Schmid, P. J., Hickel, S. & Adams, N. 2012 Analysis of unsteady behaviour in shockwave turbulent boundary layer interaction. *Journal of Fluid Mechanics* **700**, 16–28.

Jovanović, M. R., Schmid, P. J. & Nichols, J. W. 2014 Sparsity-promoting dynamic mode decomposition. *Physics of Fluids* **26** (2).

Schmid, P. J. 2010 Dynamic mode decomposition of numerical and experimental data. *Journal of Fluid Mechanics* **656**, 5–28.

Schmid, P. J., Li, L., Juniper, M. P. & Pust, O. 2011 Applications of the dynamic mode decomposition. *Theoretical and Computational Fluid Dynamics* **25** (1), 249–259.

Schreyer, A.-M, Stephan, S. & Radespiel, R. 2016*a* Characterization of the supersonic wake of a generic space launcher. *CEAS Space Journal* pp. 1–14.

Schreyer, A.-M., Stephan, S. & Radespiel, R. 2016*b* Flow structure and unsteadiness in the supersonic wake of a generic space launcher, AIAA 2016-1589.

Sirovich, L. 1987 Turbulence and the dynamics of coherent structures: Part I: Coherent structures. *Quarterly of Applied Mathematics* **XLV** (3), 561–571.

Statnikov, V., Sayadi, T., Meinke, M., Schmid, P. & Schröder, W. 2015 Analysis of pressure perturbation sources on a generic space launcher after-body in supersonic flow using zonal turbulence modeling and dynamic mode decomposition. *Physics of Fluids* **27** (1), –.

Statnikov, V., Stephan, S., Pausch, K., Meinke, M., Radespiel, R. & Schröder, W. 2016 Experimental and numerical investigations of the turbulent wake flow of a generic space launcher at \ M ∞ = 6. *CEAS Space Journal* **8** (2), 101–116.

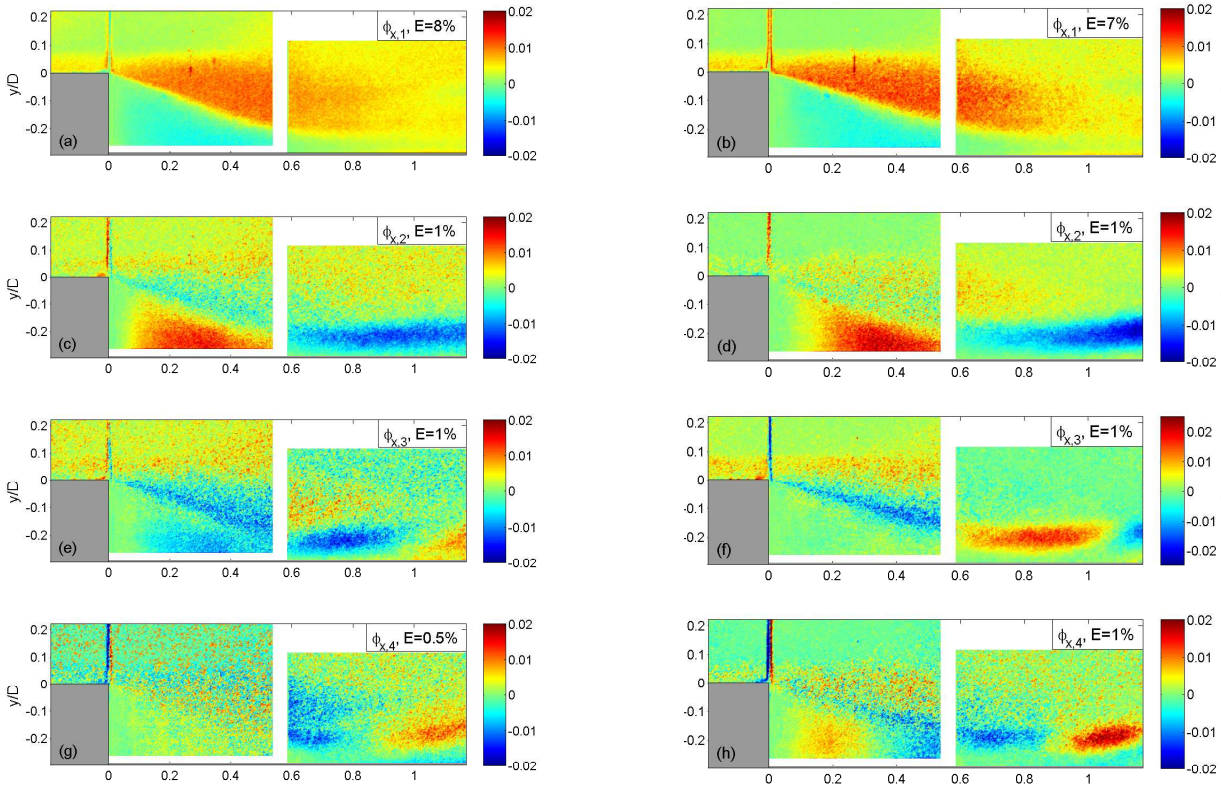

Figure 5: POD modes for streamwise velocity fluctuations $\frac{u}{U_\infty}$. Left: baseline case, right: with propulsive jet.

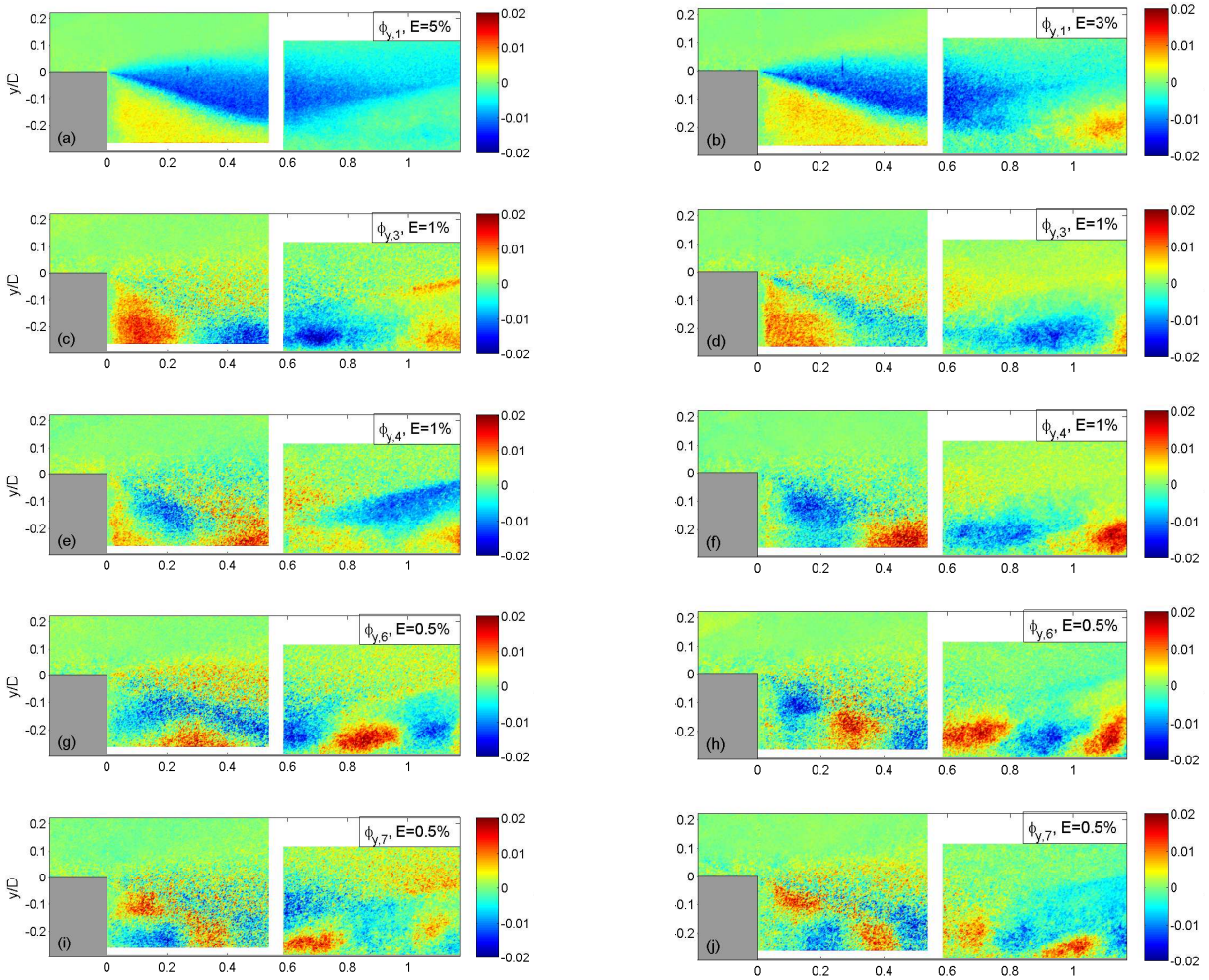

Figure 6: POD modes for velocity fluctuations in the radial direction $\frac{v}{U_\infty}$. Left: baseline case, right: with propulsive jet.

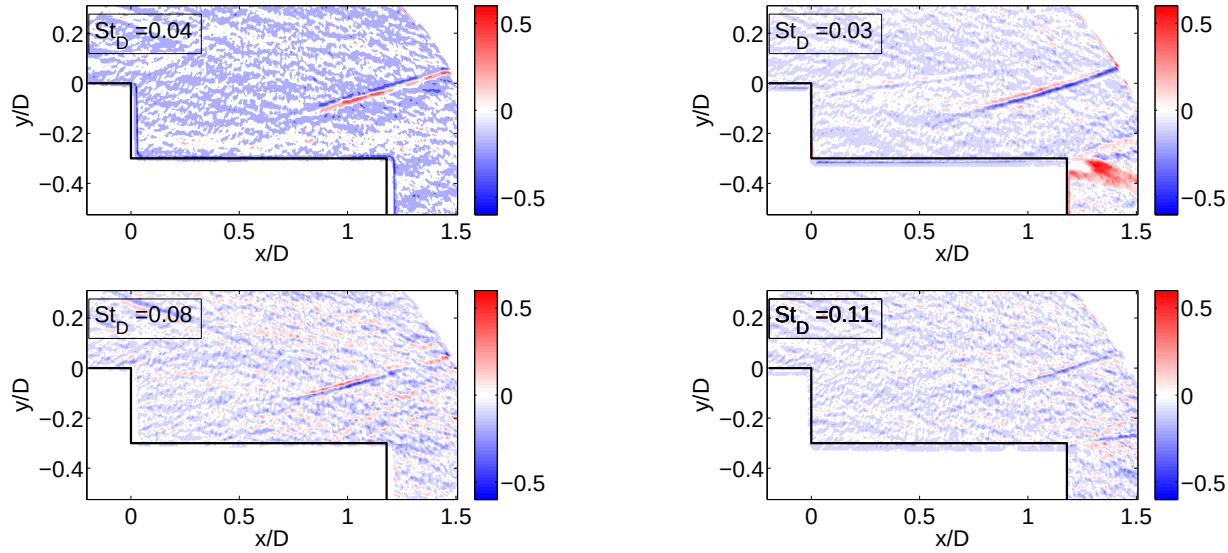

(a) Baseline case

(b) With propulsive jet

Figure 7: Exemplary dynamic modes (real part only) representative for the motion of the recompression shock.